


Article

Future X-ray Polarimetry of Relativistic Accelerators: Pulsar Wind Nebulae and Supernova Remnants

Niccolò Bucciantini ^{1,2,3} ¹ INAF—Osservatorio Astrofisico di Arcetri, Largo E. Fermi 5, I-50125 Firenze, Italy; niccolo@arcetri.astro.it² Dipartimento di Fisica e Astronomia, Università degli Studi di Firenze, Via G. Sansone 1, Sesto F. no, I-50019 Firenze, Italy³ INFN—Sezione di Firenze, Via G. Sansone 1, Sesto F. no, I-50019 Firenze, Italy

Received: 29 January 2018; Accepted: 20 March 2018; Published: date

Abstract: Supernova remnants (SNRs) and pulsar wind nebulae (PWNe) are among the most significant sources of non-thermal X-rays in the sky, and the best means by which relativistic plasma dynamics and particle acceleration can be investigated. Being strong synchrotron emitters, they are ideal candidates for X-ray polarimetry, and indeed the Crab nebula is up to present the only object where X-ray polarization has been detected with a high level of significance. Future polarimetric measures will likely provide us with crucial information on the level of turbulence that is expected at particle acceleration sites, together with the spatial and temporal coherence of magnetic field geometry, enabling us to set stronger constraints on our acceleration models. PWNe will also allow us to estimate the level of internal dissipation. I will briefly review the current knowledge on the polarization signatures in SNRs and PWNe, and I will illustrate what we can hope to achieve with future missions such as IXPE/XIPE.

Keywords: MHD; radiation mechanisms: non-thermal; polarization; relativistic processes; ISM: supernova remnants; -ISM: individual objects: Crab nebula (Please help check the keywords.)

1. Introduction

Pulsar wind nebulae (PWNe) are bubbles of relativistic particles (mostly pairs) and magnetic fields that form when the relativistic pulsar wind interacts with the ambient medium (interstellar medium (ISM) or supernova remnant (SNR)). They shine in non-thermal (synchrotron and inverse Compton) radiation in a broad range of frequencies from radio wavelengths to γ -rays (see [1] for a review). PWNe are at present one of the more promising astrophysical environments where relativistic outflows and relativistic shock acceleration can be investigated. They are, above all, one of the most efficient antimatter factories present in the galaxy and have been advocated as a possible source of the so-called “positron excess” [2,3].

At X-rays, many PWNe exhibit an axisymmetric feature known as a *jet-torus structure*. This feature has been observed by now in a number of PWNe, among which are the Crab nebula [4], Vela [5], and MSH 15-52 [6], to name just a few. It is now commonly accepted that this structure arises due to the interplay between the anisotropic energy flux in the wind and the compressed toroidal magnetic field in the nebula, as confirmed by a long series of numerical simulations [7–9], and that its shape and properties can be used to probe the structure of the otherwise unobservable pulsar wind, and the acceleration properties of the wind termination shock [10].

Shell SNRs trace the ejected layers of the parent star, launched during the supernova explosion, as they propagate into the ISM, driving a high Mach number forward shock where the ambient matter is heated and compressed, and particles are accelerated [11,12]. While the stellar ejecta are mostly revealed as thermal line emission, the forward shock is seen as a bright non-thermal limb, shining in

synchrotron from radio waves to X-rays. SNRs are commonly thought to be at the origin of the bulk of the galactic cosmic rays (CRs): diffusive shock acceleration, consisting of repeated crossings of the surface of the shock, is capable of rising the particle energy up to $\sim 0.1\text{--}1$ PeV [13].

In the last decade, it has become clear that the acceleration process can strongly modify the dynamics of the shock, and in particular can substantially amplify the magnetic field upstream of the shock itself, driving the development of magnetic turbulence [14–17]. This has crucial implications for the particle spectra and the maximum energy that can be achieved. The synchrotron X-rays seen in young SNRs are due to accelerated electrons with typical energies of 1–10 TeV in a magnetic field of a few hundred μG [15]. Such high values of the magnetic field strength cannot be explained by shock compression alone, but can be produced by instabilities in the upstream due to the accelerated particles themselves [14].

2. Radio & Optical Polarization

Radio polarimetry of PWNs and SNRs has a long history. In PWNs, as radio emission is dominated by the outer regions of the nebula, where the effects of the interaction with the SNR are stronger, and where Rayleigh–Taylor instability operates, radio polarimetry provides at best an estimate of the degree of ordered versus disordered magnetic field. This means that it cannot be used to probe the conditions in the region close to the termination shock, where most of the variability and the acceleration processes take place. In the Crab nebula, which constitutes a case study for the entire class, the radio polarized fraction is $\sim 16\%$ on average [18–21] with peaks up to 30%, which is lower than the average optical polarized fraction, which is $\sim 25\%$ [20]. Interestingly, the polarized flux in radio anti-correlates with the position of the bright X-ray torus.

In other systems, the interpretation of the radio polarized morphology can be quite challenging. Vela shows a clear toroidal pattern, consistent with the orientation of the double ring that is observed in X-rays [22]. A similar highly ordered toroidal pattern is seen also in G106.6-29 [23]. This is consistent with the general expectation of a synchrotron bubble where a highly wound-up magnetic field is inflated by the wind coming from a rapid rotator. Other systems clearly show a far more complex morphology, ranging from a highly turbulent structure [24], typical in old systems that have gone through a strong interaction phase with the SNR known as the reverberation phase [25,26], to one that is mostly radial (or dipole-like) [27]. There is at the moment no framework to interpret these differences or to relate them consistently to the dynamics of the PWNs.

For the Crab nebula, high resolution HST observations in polarized light for the inner region, in particular the brightest optical features, namely the *knot* and the *wisps*, show typical polarized fractions of about 60% and 40%, respectively [28]. The results in the Crab nebula are consistent with the general idea of a mostly toroidal magnetic field just downstream of the termination shock, with a possible hint of developing turbulence: the polarized fraction of the wisps is lower than the one in the knot, and at present, emission maps based on numerical simulations suggest that the former is slightly more downstream than the latter. It is interesting to notice that, while it is the brightest feature in total light, the torus has a lower surface brightness than the wisp in polarized light [29]. There is no optical counterpart to Vela, neither in total nor in polarized light [30,31]. As of today, optical polarization is limited to the brightest features of the brightest nebula. Moreover, the optical light usually suffers from large foreground contamination and is often polarized, and the jet-torus structure, which is substantially prominent in X-rays, is much fainter.

The radio polarization of shell SNRs shows an interesting dichotomy between young systems, where the magnetic field appears to be predominantly radial, and old systems, where it looks tangential to the shock front [32]. This is commonly interpreted as an evidence for a stronger level of instability in young and more energetic systems, more likely related to the formation of Rayleigh–Taylor fingers [33,34] at the contact discontinuity between the shocked ISM and the shocked SN ejecta, which will act to preferentially stretch the field in the radial direction. Alternative models invoking other kinds of instabilities, such as Richtmyer–Meshkov, have also been presented [35], as well as models with

magnetic dependent acceleration [36]. In older systems, where these instabilities are supposed to be less effective, the field has the naive geometry that one would expect from shock compression (note that shock compression will amplify the tangential component of the field, producing a strong polarization pattern even if the upstream field is strongly turbulent). This dichotomy appears independently of the progenitor type of the SNR.

On the other hand, there are lines of evidence suggesting that some signatures of the upstream mean field are preserved. In particular, there appears to be a correlation between the orientation of bipolar SNRs and the galactic plane [37,38], and there is further evidence in SNRs from Type II SN of an expansion into a magnetized wind bubble [39]. It was found in SN 1006 that the polarized fraction anti-correlates with radio emissions, suggesting that those sites along the shock front that are more likely to accelerate particles have a more turbulent field [38]. It is well known that the level of turbulence and the orientation of the field are pivotal for particle acceleration models: perpendicular shocks are thought to be more efficient accelerators, while parallel shocks tend to be more efficient injectors. Moreover, turbulence is likely required to explain the high magnetic field strength required in SED fitting of shell SNRs [12]. As for PWNs, radio polarization in SNRs traces particles with lifetimes that are longer than the age of the nebulae that are filling the shell volume. In Cas A, for example, high resolution radio observations show evidence of a polarization angle swing at the location of the X-ray rim, which is where particles are accelerated [40].

3. Polarization Models

In the last decade, several multidimensional models have been put forward to investigate the magnetic field structure and the geometry of the flow in PWNs. Much of the work has focused on trying to reproduce the jet-torus structure and to use it as a probe for the properties of the otherwise unobservable pulsar wind [7–9]. These works have shown the importance of Doppler boosting effects and have enabled us to locate the possible origin on many of the primary axisymmetric features observed in PWNs, including the *knot* and *wisps* of the Crab nebula. On the other hand, in present day numerical models, the torus tends to be under-luminous with respect to the wisps, and despite being a strong dynamical feature, the jet is hard to reproduce. What is missing in current day models is the possible presence of magnetic turbulence, at scales that are too small to be resolved by our numerical tools but are sufficiently large to affect emission. Several theoretical arguments suggesting that a non-negligible amount of magnetic turbulence should be present in PWNs have been put forward in recent years. For example, the presence of diffuse X-ray halos has been stated to be larger than what is expected for synchrotron cooling and advection [41–43], it has been suggested that radio-emitting particles are accelerated in the bulk of the nebula [10,44], and the recurrent γ -ray flares have been interpreted as dissipation in localized strong current sheets [45]. The possible origin of such turbulence is unclear: it could simply be the magnetic cascade of the large-scale turbulence injected at the termination shock [46]; it could be due to residual reconnection taking place downstream of the shock in a striped wind [47]; it also could be related to current-driven instability of the compressed toroidal field [48,49].

Based on the idea that small-scale turbulence can be present, we have developed a formalism to include it, as a sub-grid effect [50–52], into large scale models for the global structure of the field, either simplified toy models on the line of [53], which are easy and fast to compute and allow us to deeply scan the possible parameter space in order to optimize the agreement with observations, or more sophisticated time-dependent numerical models that can take into account the interplay between the pulsar wind and the environment. These models have been recently applied to the Crab and Vela nebulae [52]. It has been shown that, in order to recover the current-relative brightness between the wisps and torus as well as the correct luminosity profile of the torus in Crab and of the inner and outer ring in Vela, a substantial fraction of magnetic energy of $\sim 50\%$ must be in the form of a turbulent small-scale field. This number represents a typical integrated polarized fraction for the Crab nebula of $\sim 17\%$, consistent with existing measures.

SNRs have a long history of polarization models for the radio band, and such models have attempted to constrain the origin of the observed polarization dichotomy, including recipes to relate it to the physics of acceleration [15,36]. More recently, the same technique used to include the effects of a turbulent component in the emission of PWNs have been applied to shell SNRs, trying to derive possible observational constraints to locate the regions where the turbulence is higher, and to assess its correlation with particle acceleration sites [51]. One of the most interesting aspects of X-ray emission in SNRs is that it takes place close to the cut-off regime: this implies that emission tends to weigh regions of higher magnetic fields to a greater extent, and this means that large differences in the polarized emission pattern are expected for shallow vs. steep magnetic turbulent spectra. The authors of [54] have used a simplified model that takes into account the typical emissivity expected in shell SNRs, to evaluate the level and structure of polarized emission expected from different turbulent spectra, and found that even the simple detection of a polarized signal is enough to rule out the shallower cascades.

More interestingly, a polarized emission model has been recently presented to explain the striped zone observed in X-rays in Tycho SNR [55]. It has been suggested that such stripes might trace turbulent magnetic fields generated by accelerated particles streaming upstream of the the shock itself. The orientation of the magnetic field with respect to the stripes might enable us to constrain the kind of instability driving the amplification of the field, given that different mechanisms provide different polarization patterns [14,56].

4. Prospects for Future Observations

Ideally one would like to probe these systems using X-ray polarimetry [57], and there is great interest among the scientific community for such an objective [58,59]. Incidentally, the Crab nebula is at the moment the only object with a polarization detected in X-rays [60]. The Crab nebula has been more recently observed in X-ray polarized light by NuSTAR [61] and by PoGO+ [62,63]. High-energy measures by INTEGRAL are also available [64], and there are suggestions of a possible time variation in the polarization angle [65]. Recent polarized detection at high energies has also been reported by AstroSat [66].

In recent years, a renewed interest in modeling space-resolved polarimetric measures has come as a result of the great efforts made to develop the IXPE and XIPE missions [58,59]. Simulations using the baseline combined telescope effective area and point spread function (PSF) were performed for both instruments.

For Crab and Vela, IXPE will be able to measure the polarization in a number of different spatial resolution elements, thus providing the first spatially resolved X-ray polarimetry of a PWN (Figure 1). For Crab, it is estimated that a 7.3-day observation can detect a polarized fraction well below 2% at 99% confidence in each of five distinct spatial regions, including one centered on the jet. This takes into account the fact that 50% of the flux might originate in neighboring zones and be unpolarized. For Vela, a polarization of the entire nebula of 3% may be detected in a 4.6-day observation, allowing also for some spatially resolved imaging with a higher threshold of ~5–10%. For other bright PWNs powered by young pulsars such as PSR B1509-58 and J1833-1034, it will be easy with a few days of observation to have enough statistics to obtain an integrated polarized fraction and, perhaps in the case of B1509-58, to also obtain the polarization of the bright jet.

XIPE various simulations of different scenarios with magnetic field orientations based on simplified toy models [52] (see Figure 2) were carried out both for Crab and MSH 15-52 [67] and, with just a 0.2 ksec observation for Crab and a 2 Msec observation for MSH 15-52, showed that the polarized patterns are reconstructed with errors of less than 0.1% and with more than 10σ within the instrument PSF (see the contribution by J. Vink in these same proceedings for details on the modeling of these observations, the instrumental response, and the robustness of the results).

The main targets for polarization measures among shell SNRs are the few that are young and close-by, have enough surface brightness, and are large enough to be resolved. XIPE can detect polarized X-ray emission from Tycho's SNR with enough resolution to allow us to set constraints

on models of diffusive shock acceleration with efficient magnetic field amplification in SNRs, with a typical integration time of ~ 1 Msec. In Tycho, the emission in the 4–6 keV range is expected to be of synchrotron origin. The current Monte Carlo method of constructing simulated observations are based on theoretical models for polarized emission constructed by [67].

Another primary target among SNRs will be Cas A, where thermal line emission associated with the interior filaments is present. A good energy resolution is pivotal to select those parts of the emitted X-ray radiation that are of non-thermal origin (far from the lines). In Cas A, X-ray emission is detected also from the putative reverse shock. Simulated observations suggest that, with XIPE, it is possible to disentangle the polarization signature of the reverse shock from that of the forward shock, as long as typical values are $\sim 10\%$ (see the contribution by J. Vink in these same proceedings). Among other possible targets, there are SN 1006, RX J1713.7-394, Kepler's SNR, and RCW 86.

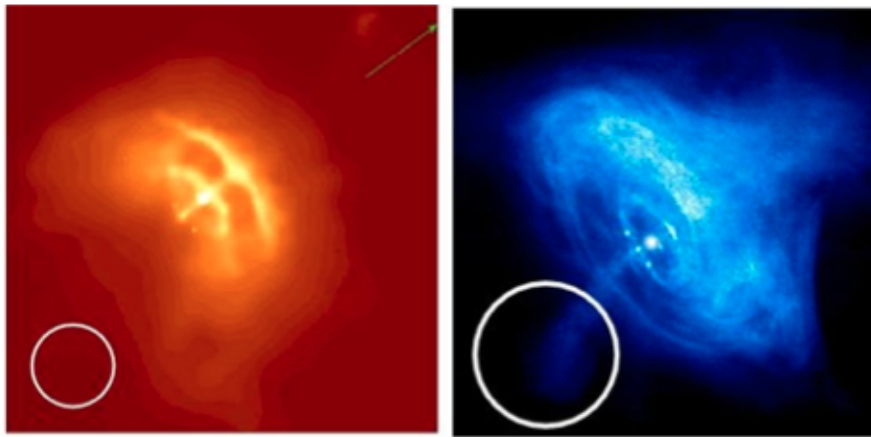


Figure 1. Chandra images of the Vela (left) and Crab (right) PWNs. The IXPE 30'' resolution (half power diameter) is shown in the lower left corners of the images. From the IXPE Science-Investigation Document.

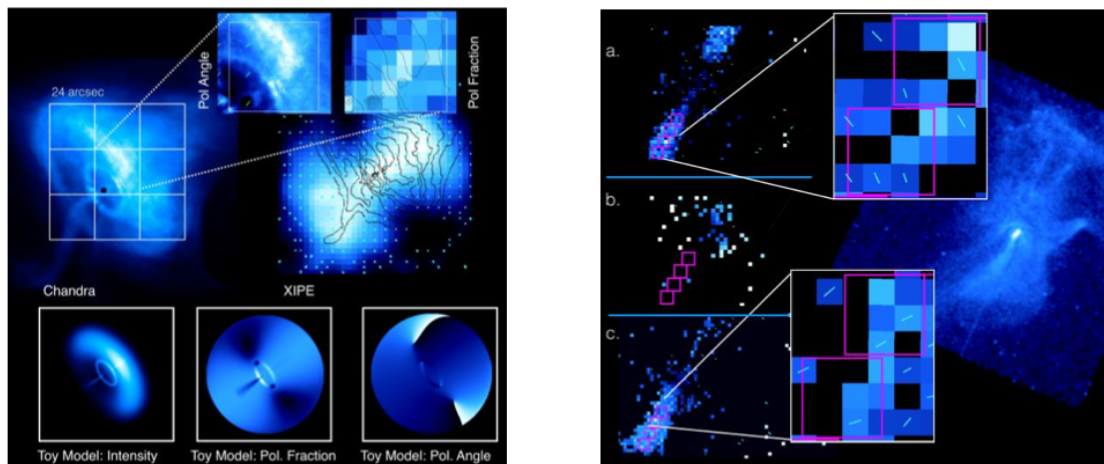


Figure 2. Left panel (a): Simulation of the Crab Nebula as seen by XIPE in 0.2 Msec. The toy model mimics the Chandra image for a given polarization angle and fraction. Right panel (b): Simulations of the PWN MSH 15-52 as seen by XIPE in 2 Msec. The images a, b, and c show the expected intensity map when three different polarization models are applied to the Chandra intensity map: (a) a fully ordered radial B-field, (b) a fully disordered B-field, and (c) a fully ordered perpendicular B-field. From the XIPE Yellow Book, see also [67].

Conflicts of Interest: The authors declare no conflicts of interest. (Please confirm the conflict of interest.)

References

1. Gaensler, B.M.; Slane, P.O. The Evolution and Structure of Pulsar Wind Nebulae. *Annu. Rev. Astron. Astrophys.* **2006**, *44*, 17–47.
2. Adriani, O.; Barbarino, G.C.; Bazilevskaya, G.A.; Bellotti, R.; Boezio, M.; Bogomolov, E.A.; Bonechi, L.; Bongi, M.; Bonvicini, V.; Bottai, S.; et al. An anomalous positron abundance in cosmic rays with energies 1.5–100 GeV. *Nature* **2009**, *458*, 607–609.
3. Blasi, P.; Amato, E. Positrons from pulsar winds. *Astrophys. Space Sci. Proc.* **2011**, *21*, 623–641.
4. Weisskopf, M.C.; Hester, J.J.; Tennant, A.F.; Elsner, R.F.; Schulz, N.S.; Marshall, H.L.; Karovska, M.; Nichols, J.S.; Swartz, D.A.; Kolodziejczak, J.J.; et al. Discovery of Spatial and Spectral Structure in the X-Ray Emission from the Crab Nebula. *Astrophys. J. Lett.* **2000**, *536*, L81–L84.
5. Pavlov, G.G.; Kargaltsev, O.Y.; Sanwal, D.; Garmire, G.P. Variability of the Vela Pulsar Wind Nebula Observed with Chandra. *Astrophys. J. Lett.* **2001**, *554*, L189–L192.
6. Gaensler, B.M.; Arons, J.; Kaspi, V.M.; Pivovarov, M.J.; Kawai, N.; Tamura, K. Chandra Imaging of the X-Ray Nebula Powered by Pulsar B1509–58. *Astrophys. J.* **2002**, *569*, 878–893.
7. Komissarov, S.S.; Lyubarsky, Y.E. Synchrotron nebulae created by anisotropic magnetized pulsar winds. *Mon. Not. R. Astron. Soc.* **2004**, *349*, 779–792.
8. Del Zanna, L.; Amato, E.; Bucciantini, N. Axially symmetric relativistic MHD simulations of Pulsar Wind Nebulae in Supernova Remnants. On the origin of torus and jet-like features. *Astron. Astrophys.* **2004**, *421*, 1063–1073.
9. Olmi, B.; Del Zanna, L.; Amato, E.; Bucciantini, N.; Mignone, A. Multi-D magnetohydrodynamic modelling of pulsar wind nebulae: Recent progress and open questions. *J. Plasma Phys.* **2016**, *82*, 635820601.
10. Olmi, B.; Del Zanna, L.; Amato, E.; Bucciantini, N. Constraints on particle acceleration sites in the Crab nebula from relativistic magnetohydrodynamic simulations. *Mon. Not. R. Astron. Soc.* **2015**, *449*, 3149–3159.
11. Woltjer, L. Supernova Remnants. *Annu. Rev. Astron. Astrophys.* **1972**, *10*, 129–158.
12. Reynolds, S.P. Supernova Remnants at High Energy. *Annu. Rev. Astron. Astrophys.* **2008**, *46*, 89–126.
13. Reynolds, S.P. Particle acceleration in supernova-remnant shocks. *Astrophys. Space Sci.* **2011**, *336*, 257–262.
14. Bell, A.R. Turbulent amplification of magnetic field and diffusive shock acceleration of cosmic rays. *Mon. Not. R. Astron. Soc.* **2004**, *353*, 550–558.
15. Reynolds, S.P.; Gaensler, B.M.; Bocchino, F. Magnetic Fields in Supernova Remnants and Pulsar-Wind Nebulae. *Space Sci. Rev.* **2012**, *166*, 231–261.
16. Matthews, J.H.; Bell, A.R.; Blundell, K.M.; Araudo, A.T. Amplification of perpendicular and parallel magnetic fields by cosmic ray currents. *Mon. Not. R. Astron. Soc.* **2017**, *469*, 1849–1860.
17. Xu, S.; Lazarian, A. Magnetic Field Amplification in Supernova Remnants. *Astrophys. J.* **2017**, *850*, 126.
18. Conway, R.G. Radio Polarization of the Crab Nebula. In *The Crab Nebula, Proceedings of the International Astronomical Union / Union Astronomique Internationale (Symposium No. 46)*, Jodrell Bank, UK, 5–7 August 1970; Davies, R.D., Graham-Smith, F., Eds.; Springer: Dordrecht, The Netherlands, 1971; p. 292.
19. Ferguson, D.C. A Comparison of the Optical and Radio Polarization of the Crab Nebula Pulsar. *Bull. Am. Astron. Soc.* **1973**, *5*, 425.
20. Velusamy, T. Structure of the Crab Nebula—Intensity and polarization at 20 CM. *Mon. Not. R. Astron. Soc.* **1985**, *212*, 359–365.
21. Aumont, J.; Conversi, L.; Thum, C.; Wiesemeyer, H.; Falgarone, E.; Macías-Pérez, J.F.; Piacentini, F.; Pointecouteau, E.; Ponthieu, N.; Puget, J.L.; et al. Measurement of the Crab nebula polarization at 90 GHz as a calibrator for CMB experiments. *Astron. Astrophys.* **2010**, *514*, A70.
22. Dodson, R.; Lewis, D.; McConnell, D.; Deshpande, A.A. The radio nebula surrounding the Vela pulsar. *Mon. Not. R. Astron. Soc.* **2003**, *343*, 116–124.
23. Kothes, R.; Reich, W.; Uyaniker, B. The Boomerang PWN G106.6+2.9 and the Magnetic Field Structure in Pulsar Wind Nebulae. *Astrophys. J.* **2006**, *638*, 225–233.
24. Ma, Y.K.; Ng, C.Y.; Bucciantini, N.; Slane, P.O.; Gaensler, B.M.; Temim, T. Radio Polarization Observations of the Snail: A Crushed Pulsar Wind Nebula in G327.1-1.1 with a Highly Ordered Magnetic Field. *Astrophys. J.* **2016**, *820*, 100.
25. Blondin, J.M.; Chevalier, R.A.; Frierson, D.M. Pulsar Wind Nebulae in Evolved Supernova Remnants. *Astrophys. J.* **2001**, *563*, 806–815.

26. Bucciantini, N.; Blondin, J.M.; Del Zanna, L.; Amato, E. Spherically symmetric relativistic MHD simulations of pulsar wind nebulae in supernova remnants. *Astron. Astrophys.* **2003**, *405*, 617–626.
27. Kothes, R.; Landecker, T.L.; Reich, W.; Safi-Harb, S.; Arzoumanian, Z. DA 495: An Aging Pulsar Wind Nebula. *Astrophys. J.* **2008**, *687*, 516–531.
28. Moran, P.; Shearer, A.; Mignani, R.P.; Slowikowska, A.; De Luca, A.; Gouiffès, C.; Laurent, P. Optical polarimetry of the inner Crab nebula and pulsar. *Mon. Not. R. Astron. Soc.* **2013**, *433*, 2564–2575.
29. Hester, J.J. The Crab Nebula: An Astrophysical Chimera. *Annu. Rev. Astron. Astrophys.* **2008**, *46*, 127–155.
30. Marubini, T.E.; Sefako, R.R.; Venter, C.; de Jager, O.C. A search for optical counterparts of the complex Vela X system. *arXiv* **2015**, arXiv:1501.00278.
31. Moran, P.; Mignani, R.P.; Shearer, A. HST optical polarimetry of the Vela pulsar and nebula. *Mon. Not. R. Astron. Soc.* **2014**, *445*, 835–844.
32. Dubner, G.; Giacani, E. Radio emission from supernova remnants. *Astron. Astrophys. Rev.* **2015**, *23*, 3.
33. Jun, B.I. Interaction of a Pulsar Wind with the Expanding Supernova Remnant. *Astrophys. J.* **1998**, *499*, 282–293.
34. Bucciantini, N.; Amato, E.; Bandiera, R.; Blondin, J.M.; Del Zanna, L. Magnetic Rayleigh-Taylor instability for Pulsar Wind Nebulae in expanding Supernova Remnants. *Astron. Astrophys.* **2004**, *423*, 253–265.
35. Inoue, T.; Shimoda, J.; Ohira, Y.; Yamazaki, R. The Origin of Radially Aligned Magnetic Fields in Young Supernova Remnants. *Astrophys. J. Lett.* **2013**, *772*, L20.
36. West, J.L.; Jaffe, T.; Ferrand, G.; Safi-Harb, S.; Gaensler, B.M. When Disorder Looks Like Order: A New Model to Explain Radial Magnetic Fields in Young Supernova Remnants. *Astrophys. J. Lett.* **2017**, *849*, L22.
37. Gaensler, B.M. The Nature of Bilateral Supernova Remnants. *Astrophys. J.* **1998**, *493*, 781–792.
38. Reynoso, E.M.; Hughes, J.P.; Moffett, D.A. On the Radio Polarization Signature of Efficient and Inefficient Particle Acceleration in Supernova Remnant SN 1006. *Astron. J.* **2013**, *145*, 104.
39. Harvey-Smith, L.; Gaensler, B.M.; Kothes, R.; Townsend, R.; Heald, G.H.; Ng, C.Y.; Green, A.J. Faraday Rotation of the Supernova Remnant G296.5+10.0: Evidence for a Magnetized Progenitor Wind. *Astrophys. J.* **2010**, *712*, 1157–1165.
40. Gotthelf, E.V.; Koralesky, B.; Rudnick, L.; Jones, T.W.; Hwang, U.; Petre, R. Chandra Detection of the Forward and Reverse Shocks in Cassiopeia A. *Astrophys. J. Lett.* **2001**, *552*, L39–L43.
41. Tang, X.; Chevalier, R.A. Particle Transport in Young Pulsar Wind Nebulae. *Astrophys. J.* **2012**, *752*, 83.
42. Bühler, R.; Blandford, R. The surprising Crab pulsar and its nebula: A review. *Rep. Prog. Phys.* **2014**, *77*, 066901.
43. Zrake, J.; Arons, J. Turbulent Magnetic Relaxation in Pulsar Wind Nebulae. *Astrophys. J.* **2017**, *847*, 57.
44. Tanaka, S.J.; Asano, K. On the Radio-emitting Particles of the Crab Nebula: Stochastic Acceleration Model. *Astrophys. J.* **2017**, *841*, 78.
45. Uzdensky, D.A.; Cerutti, B.; Begelman, M.C. Reconnection-powered Linear Accelerator and Gamma-Ray Flares in the Crab Nebula. *Astrophys. J. Lett.* **2011**, *737*, L40.
46. Camus, N.F.; Komissarov, S.S.; Bucciantini, N.; Hughes, P.A. Observations of ‘wisps’ in magnetohydrodynamic simulations of the Crab Nebula. *Mon. Not. R. Astron. Soc.* **2009**, *400*, 1241–1246.
47. Sironi, L.; Spitkovsky, A. Acceleration of Particles at the Termination Shock of a Relativistic Striped Wind. *Astrophys. J.* **2011**, *741*, 39.
48. Mizuno, Y.; Lyubarsky, Y.; Nishikawa, K.I.; Hardee, P.E. Three-dimensional Relativistic Magnetohydrodynamic Simulations of Current-driven Instability. II. Relaxation of Pulsar Wind Nebula. *Astrophys. J.* **2011**, *728*, 90.
49. O’Neill, S.M.; Beckwith, K.; Begelman, M.C. Local simulations of instabilities in relativistic jets—I. Morphology and energetics of the current-driven instability. *Mon. Not. R. Astron. Soc.* **2012**, *422*, 1436–1452.
50. Bandiera, R.; Petruk, O. Radio polarization maps of shell-type supernova remnants—I. Effects of a random magnetic field component and thin-shell models. *Mon. Not. R. Astron. Soc.* **2016**, *459*, 178–198.
51. Petruk, O.; Bandiera, R.; Beshley, V.; Orlando, S.; Miceli, M. Radio polarization maps of shell-type SNRs—II. Sedov models with evolution of turbulent magnetic field. *Mon. Not. R. Astron. Soc.* **2017**, *470*, 1156–1176.
52. Bucciantini, N.; Bandiera, R.; Olmi, B.; Del Zanna, L. Modeling the effect of small-scale magnetic turbulence on the X-ray properties of Pulsar Wind Nebulae. *Mon. Not. R. Astron. Soc.* **2017**, *470*, 4066–4074.
53. Ng, C.Y.; Romani, R.W. Fitting Pulsar Wind Tori. *Astrophys. J.* **2004**, *601*, 479–484.

54. Bykov, A.M.; Uvarov, Y.A.; Bloemen, J.B.G.M.; den Herder, J.W.; Kaastra, J.S. A model of polarized X-ray emission from twinkling synchrotron supernova shells. *Mon. Not. R. Astron. Soc.* **2009**, *399*, 1119–1125.
55. Bykov, A.M.; Ellison, D.C.; Osipov, S.M.; Pavlov, G.G.; Uvarov, Y.A. X-ray Stripes in Tycho's Supernova Remnant: Synchrotron Footprints of a Nonlinear Cosmic-ray-driven Instability. *Astrophys. J. Lett.* **2011**, *735*, L40.
56. Bykov, A.M.; Osipov, S.M.; Ellison, D.C. Cosmic ray current driven turbulence in shocks with efficient particle acceleration: The oblique, long-wavelength mode instability. *Mon. Not. R. Astron. Soc.* **2011**, *410*, 39–52.
57. Bucciantini, N. Polarization of pulsar wind nebulae. In *X-ray Polarimetry: A New Window in Astrophysics by Ronaldo Bellazzini, Enrico Costa, Giorgio Matt and Gianpiero Tagliaferri*; Bellazzini, R., Costa, E., Matt, G., Tagliaferri, G., Eds.; Cambridge University Press: Cambridge, UK, 2010; p. 195.
58. Soffitta, P.; Barcons, X.; Bellazzini, R.; Braga, J.; Costa, E.; Fraser, G.W.; Gburek, S.; Huovelin, J.; Matt, G.; Pearce, M.; et al. XIPE: The X-ray imaging polarimetry explorer. *Exp. Astron.* **2013**, *36*, 523–567.
59. Weisskopf, M.C.; Ramsey, B.; O'Dell, S.; Tennant, A.; Elsner, R.; Soffitta, P.; Bellazzini, R.; Costa, E.; Kolodziejczak, J.; Kaspi, V.; et al. The Imaging X-ray Polarimetry Explorer (IXPE). In Proceedings of the Space Telescopes and Instrumentation 2016: Ultraviolet to Gamma Ray, Edinburgh, UK, 26 June–1 July 2016.
60. Weisskopf, M.C.; Silver, E.H.; Kestenbaum, H.L.; Long, K.S.; Novick, R. A precision measurement of the X-ray polarization of the Crab Nebula without pulsar contamination. *Astrophys. J. Lett.* **1978**, *220*, L117–L121.
61. Madsen, K.K.; Reynolds, S.; Harrison, F.; An, H.; Boggs, S.; Christensen, F.E.; Craig, W.W.; Fryer, C.L.; Grefenstette, B.W.; Hailey, C.J.; et al. Broadband X-ray Imaging and Spectroscopy of the Crab Nebula and Pulsar with NuSTAR. *Astrophys. J.* **2015**, *801*, 66.
62. Chauvin, M.; Florén, H.G.; Jackson, M.; Kamae, T.; Kawano, T.; Kiss, M.; Kole, M.; Mikhalev, V.; Moretti, E.; Olofsson, G.; et al. Observation of polarized hard X-ray emission from the Crab by the PoGOLite Pathfinder. *Mon. Not. R. Astron. Soc.* **2016**, *456*, L84–L88.
63. Chauvin, M.; Florén, H.G.; Friis, M.; Jackson, M.; Kamae, T.; Kataoka, J.; Kawano, T.; Kiss, M.; Mikhalev, V.; Mizuno, T.; et al. Shedding new light on the Crab with polarized X-rays. *Sci. Rep.* **2017**, *7*, 7816.
64. Forot, M.; Laurent, P.; Grenier, I.A.; Gouiffès, C.; Lebrun, F. Polarization of the Crab Pulsar and Nebula as Observed by the INTEGRAL/IBIS Telescope. *Astrophys. J. Lett.* **2008**, *688*, L29.
65. Moran, P.; Kyne, G.; Gouiffès, C.; Laurent, P.; Hallinan, G.; Redfern, R.M.; Shearer, A. A recent change in the optical and γ -ray polarization of the Crab nebula and pulsar. *Mon. Not. R. Astron. Soc.* **2016**, *456*, 2974–2981.
66. Vadawale, S.V.; Chattopadhyay, T.; Mithun, N.P.S.; Rao, A.R.; Bhattacharya, D.; Vibhute, A.; Bhalerao, V.B.; Dewangan, G.C.; Misra, R.; Paul, B.; et al. Phase-resolved X-ray polarimetry of the Crab pulsar with the AstroSat CZT Imager. *Nat. Astron.* **2018**, *2*, 50–55.
67. de Ona Wilhelmi, E.; Vink, J.; Bykov, A.; Zanin, R.; Bucciantini, N.; Amato, E.; Bandiera, R.; Olmi, B.; Uvarov, Y.; XIPE Science Working Group. Unveiling the magnetic structure of VHE SNRs/PWNe with XIPE, the x-ray imaging-polarimetry explorer. In Proceedings of the 6th International Symposium on High Energy Gamma-Ray Astronomy, Heidelberg, Germany, 11–15 July 2016.

